Fusion of Individual and Population Graphs in a GNN Brain Disease Network

Chunyu Hao, Xiaoying Song*, Fang Yang, Wanning Zheng, and Yufeng Zhou
School of Information Science and Engineering
Wuhan University of Science and Technology
Wuhan, China
Email: xiaoying811@wust.edu.cn

***Abstract*—In brain disease research, despite the increasing sophistication of existing graph neural network approaches, it is still a challenge to simultaneously analyse abnormal brain regions associated with diseases and to consider inter-subject relationships to improve the accuracy of disease diagnosis. In this paper, we propose a new graph neural network model for brain disease analysis by fusing information from individual and population graphs. The model designs an individual graph coarsening network to learn the most discriminative features to construct the population graph and identify abnormal brain regions. The individual graph data are fused into the population graph, and then a population hierarchical graph convolutional neural network is constructed to learn the relationship between different subjects and fully integrate the global information. Experimental results show that the proposed method achieves good classification accuracy while identifying the most discriminative brain regions, providing interpretable analyses for the study of brain diseases.**

***Index Terms*—graph neural network, fusion, individual graph, population graph, IPGNN, AD patients**

I. Introduction

Neuroimaging techniques can provide a deeper understanding of the pathological basis of neurological diseases such as Alzheimer's disease. The most widely used functional magnetic resonance imaging (fMRI) is a non-invasive imaging technique that studies the functional activity of the brain through the measurement of blood oxygen level dependence (BOLD). In particular, resting-state fMRI BOLD signals can be used to reveal abnormal brain activity in the resting state.

Currently, methods based on graph neural network (GNN), such as graph convolution network (GCN) [1], graph attention network (GAT) [2], provide new perspectives for studying brain disease issues. Work on GNN-based brain network analysis can be divided into two main categories: one is based on individual graphs [3], [4], and the other is based on population graphs [5]–[7]. In the individual graph-based brain network construction method, nodes represent brain regions of interest (ROIs) and edges represent functional connections between ROIs. Individual graphs focus on correlations between brain regions while ignoring correlations between subjects. In population graph-based brain network construction methods, nodes represent subjects and edges represent correlations between subjects, which are usually described by pairs of imaging features or phenotypic data (e.g., age, gender, genes). Population graphs focus on correlations between subjects but fail to describe the brain structure of individual subjects, making it difficult to perform interpretable analysis. In addition, many brain network structures give more attention to topology and ignore the construction of edge weights.

In order to exploit both the inter-subject correlation and the connectivity between brain regions of each subject, we propose a new graph neural network, the individual population graph neural network (IPGNN), by fusing individual and population graphs. Further, we also combine the advantages of different networks in the construction of IPGNN. We first learn the most discriminative brain regions (which can be used as biomarkers of diseases) based on the individual GNN, and later construct a population graph based on the features obtained from the individual GNN. A hierarchical GCN is constructed based on the population graph to capture the features of nodes at different levels and perform high-performance classification of brain diseases by fully integrating the global information. Our proposed IPGNN network improves the classification performance while identifying the most discriminative brain regions and mapping them to neurobiological findings, providing interpretable analyses for brain disease research.

The rest of this paper is organised as follows. Section II introduces our proposed graph neural network architecture based on the fusion of individual graph and population graph. Section III gives the classification experiment of the proposed model IPGNN applied to the ADNI dataset and performs abnormal brain area analysis. The conclusion of this paper is given in Section IV.

II. METHOD

The overall framework of the IPGNN network proposed in this paper is shown in Fig. 1. Based on the preprocessed fMRI BOLD signal, an individual graph with brain regions as nodes is constructed for each subject. Coarse features are generated using the individual graph coarsening network, and the coarse features of each subject are embedded as node (subject) features of the population graph. Further, calculate the higher-order functional connectivity (HOFC) [8] graph metric of BOLD signals to obtain the edge weights of the population graph. The hierarchical graph convolutional neural network is constructed based on the population graph to achieve the classification and prediction of subjects. The construction of

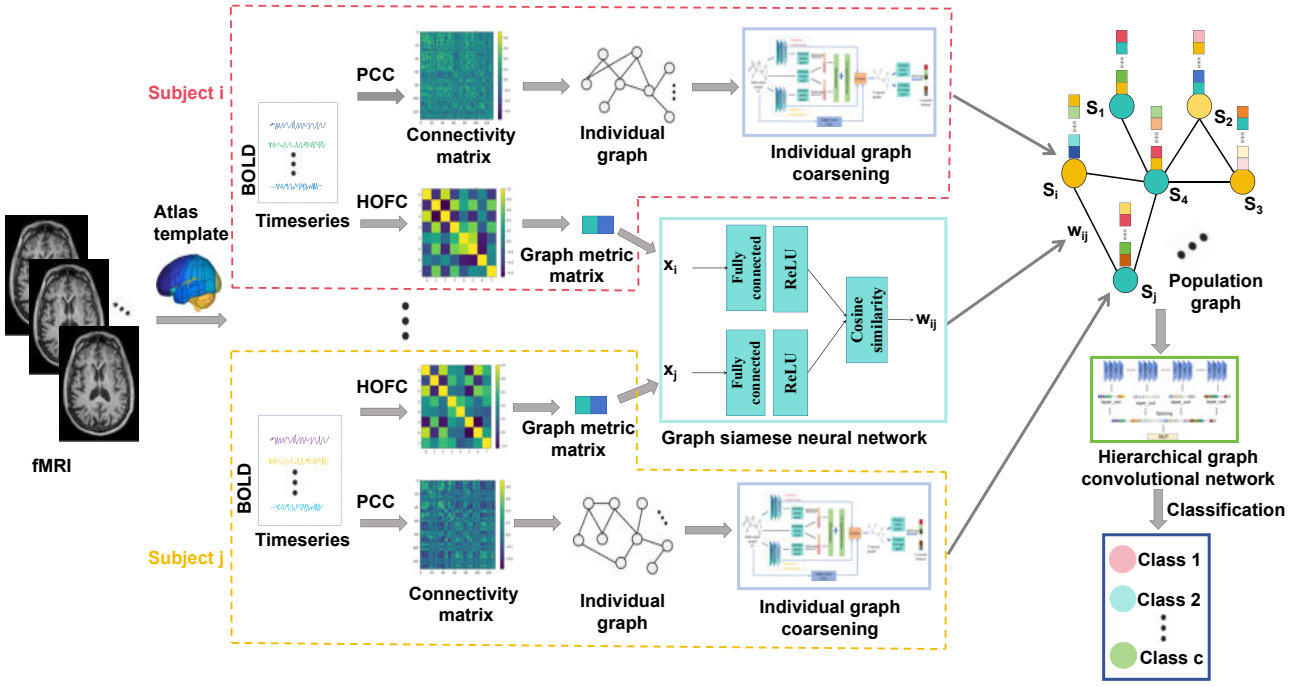

Fig. 1: The overall framework of the proposed IPGNN.

the IPGNN network is described in detail in the following subsections.

A. Individual Graph Construction

The construction of individual graph is crucial for subsequent network learning. Given an individual graph $G_1(V_1, E_1, W_1)$, V_1 represents the set of nodes, each node represents a brain region (ROI), and the number of nodes is $N = |V_1|$. $W_1 = \{w_{ij}|i,j \in V_1\} \in R^{N\times N}$ represents the weighted adjacency matrix, which is obtained from the Pearson correlation of BOLD time series between ROIs. E_1 is the set of edges such that $e_{ij} = 1$ when w_{ij} is greater than a threshold τ , indicating that there is an edge between v_i and v_j. When w_{ij} is less that the threshold τ , $e_{ij} = 0$, indicating there is no edge between v_i and v_j. The node feature matrix of G_1 is represented by $X_1 \in R^{N\times d}$, where d is the feature dimension.

B. Individual Graph Coarsening

The individual graph coarsening model is shown in Fig. 2. We use positive and negative coarsening modules on the input individual graph G_1 to obtain real and false coarsening graphs, which are used as positive and negative samples for comparative learning. This allows obtaining the most important node features in the individual graph G_1, reducing the output embedding size of the individual graph, as well as improving the robustness of the model. The coarsening network is improved based on CGIPool [9].

In the positive and negative coarsening module, we calculate the 1D attention score vector of each node in the input individual graph G_1 through two parallel graph attention networks and a multi-head attention mechanism. The positive coarsening module selects the node indexes of the top k important nodes based on the real sample score vector $y_r^{'}$ to form a real coarsening graph $G_{1r}^{'}$ that represents G_1 to the greatest extent. The negative coarsening module generates a false coarsening graph $G_{1f}^{'}$ containing the unimportant nodes in G_1 based on the negative sample score vector $y_f^{'}$. We use the edge selection mechanism in the attention network to compute the edge importance score vector y_e for edges in G_1. Then, we define the fusion score $y_d^{'}$ of the nodes and select the top k ranked nodes to construct the coarsened graph $G_1^{'}$.

$$y_d^{'} = \sigma(y_r^{'} - y_f^{'}) + y_e. \tag{1}$$

With the global mean pooling function in the weight sharing encoder network, G_1, $G_{1r}^{'}$ and $G_{1f}^{'}$ are mapped to their feature vectors $g \in R^t$, $g_r^{'} \in R^t$ and $g_f^{'} \in R^t$, respectively. By minimizing the following mutual information loss function L_{MI}, the mutual information between each pooling layer input and the coarsened graph can be maximized. In addition, the addition of a regularized loss function prevents the generation of over-fitting, thus further improving the performance of graph representation learning:

$$L_{MI} = -\frac{1}{M}\sum_{i=1}^{M}[[\log\sigma(T_d(g_i, g_{r,i}^{'})) + \log(1-\sigma(T_d(g_i, g_{f,i}^{'}))]+ \frac{\lambda}{2}\sum_p\sum_q\theta_{pq}^2] \tag{2}$$

where M is the number of subjects in the data set, σ is the sigmoid function, T_d is the discriminator network, λ is

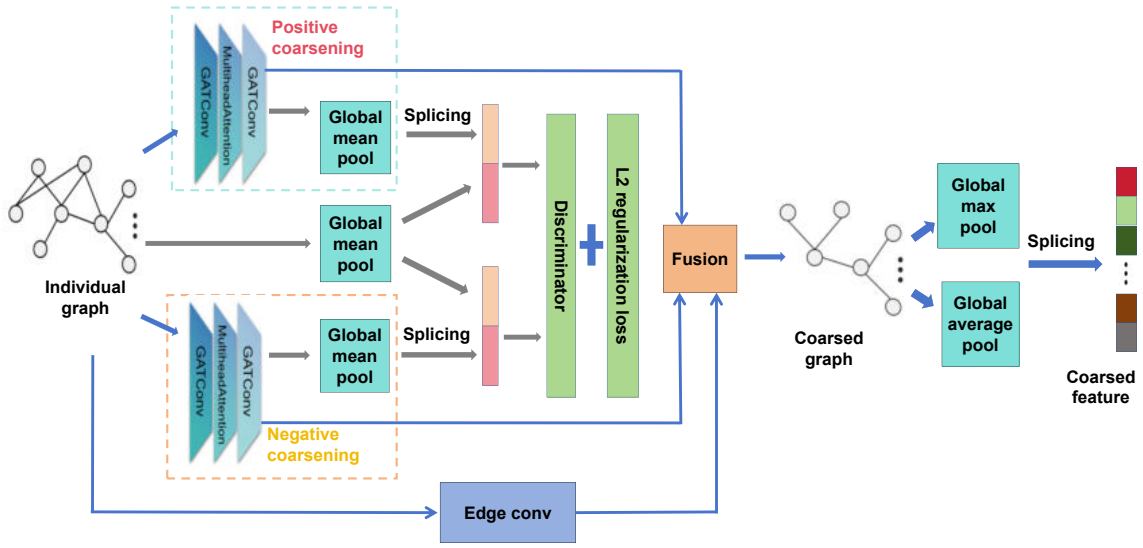

Fig. 2: Individual graph coarsening module.

the regularization coefficient (weight decay), and θ are the parameters of the model.

Since global pooling takes into account the features of the graph, we perform global maximum pooling and global average pooling on the coarsened graph, and then splice along the feature dimensions (columns) to obtain individual graph coarsened features.

C. Population Graph Construction

Considering the similarity between subjects, we then construct the population graph $G_2(V_2, E_2, W_2)$ with node set $V_2 = \{v_1, v_2, \cdots, v_M\}$ and edge set E_2. There are M nodes, each node represents a subject, and the features on the nodes are coarsened features obtained from the individual graph coarsening network. We use HOFC to construct the topological connection of G_2, that is, design W_2, which we describe in detail next. Define diagonal matrix $D := diag(d_i)$, where $d_i = \sum_j w_{ij}$ is the degree of the vertex v_i.

HOFC can be used to describe more advanced structures in complex networks and has proven to be a useful complement to brain functional connectivity. We construct the HOFC by the following steps:

1) Calculate the functional connectivity matrix $\{W_{11}, W_{12}, \cdots, W_{1M}\}$ for M subjects. Stack them to obtain the matrix $B = [W_{11}; W_{12}; \cdots; W_{1M}] \in R^{NM \times N}$.

2) Let b_j denote the jth column of B, $j = 1, 2, ..., N$. Calculate the Pearson correlation between b_i and b_j to obtain the correlation matrix $Q \in R^{N \times N}$.

3) Perform K-mean clustering on Q to classify N brain regions into K clusters. Let $\{s_j = k, j = 1, 2, \cdots, N; k = 1, 2, \cdots, K\}$ denotes the cluster to which the jth brain region belongs.

4) For jth subject, based on the clustering results, rearrange W_{1j} as $P = [P_1, P_2, \cdots, P_k, \cdots, P_K] \in R^{N \times N}$, where P_k is the concatenation of columns with the same cluster labels. Compute the mean for each cluster: $F_k = \frac{1}{\text{count}(s_j=k)} \sum P_k$ and get the rearranged functional connectivity matrix of the brain network $F = [F_1, F_2, ..., F_K] \in R^{N \times K}$. Calculate the Pearson correlation for each column in F to obtain the final HOFC matrix $Z_j \in R^{K \times K}$.

Considering Z_j of the jth subject as an adjacency matrix of a graph structure, two graph metrics, node degree D_{deg} and local efficiency E_{local}, are computed as the feature $x_j = [D_{deg}, E_{local}]$ on this node v_j. We refer to x_j as the HOFC feature, which is subsequently used to construct the edge weights of the population graph G_2.

To design the edge weight w_{ij} between nodes v_i and v_j of G_2, we input x_i and x_j into the graph siamese neural network. To prevent gradient vanishing during network training, these two feature vectors are first normalized and rescaled to unit norm vectors $\tilde{x}_i$ and $\tilde{x}_j$, respectively. Two fully connected layers with shared weights encode $\tilde{x}_i$ and $\tilde{x}_j$ in parallel as h_i and h_j,

$$\begin{aligned} h_i &= \sigma(\Omega \tilde{x}_i + b), \\ h_j &= \sigma(\Omega \tilde{x}_j + b), \end{aligned} \tag{3}$$

where σ is the activation function, Ω is the trainable weight in the fully connected layer, and b is the bias term.

Mapping h_i and h_j to a common potential space and then applying cosine similarity to compute the similarity between these two subjects, we get the following w_{ij} with values between [0,1].

$$w_{ij} = \left(\frac{{h_i}^T h_j}{||h_i|| ||h_j||} + 1\right) \times 0.5. \tag{4}$$

Performing the same operation for all subject pairs, we eventually obtain the weight matrix W_2 for G_2, and complete the construction of G_2. In our experiments, each fully

connected layer contains 128 hidden units, and we use the $ReLU$ nonlinear activation function. In addition, we introduce dropout regularization to enhance the generalisation ability and stability of the model and effectively avoid overfitting.

D. Population Graph Hierarchical GCN

The problem of over-smoothing due to too many layers of aggregation/propagation steps produces indistinguishable node representations, which degrades model performance and increases computational complexity. As a result, GCN models are usually limited to shallow architectures, yet shallow embeddings may not be able to propagate node features sufficiently to fuse heterogeneous information [10]. To address this problem, we propose a hierarchical graph convolution network, as shown in Fig. 3. The multi-layer graph convolutional layers help to capture node features at different scales, and the convolutional outputs of each layer are batch normalized and activated by the $ReLU$ function, which greatly enhances the nonlinear representation of the model.

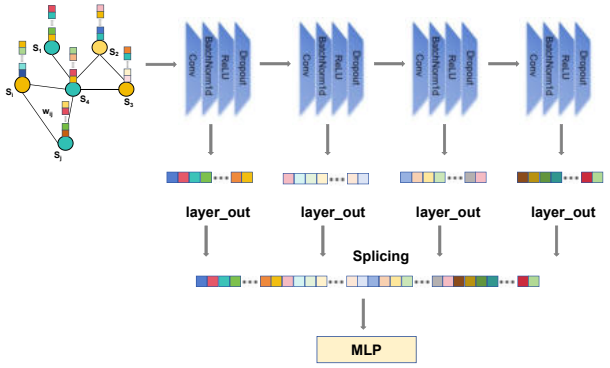

Fig. 3: Hierarchical graph convolutional network module.

To improve the learning performance of the network, we introduce ChebConv in GCN to complete the graph convolution operation, the improved graph convolution operation is as follows:

$$H^{l+1} = \sigma(U g_\theta(\Lambda) U^T H^l), \tag{5}$$

where H^l is the feature vector of the lth graph convolution layer. $L = I - D^{-\frac{1}{2}} W_2 D^{-\frac{1}{2}}$ is the Laplacian matrix of G_2 whose eigenvalue decomposition is $L = U\Lambda U^T$. $g_\theta(\Lambda)$ is the convolution kernel which is implemented by the following Chebyshev kernel:

$$g_\theta(\Lambda) = \sum_{k=0}^{K-1} \beta_k T_k(\tilde{\Lambda}), \tag{6}$$

where $T_k(\cdot)$ is the kth order Chebyshev polynomial, β_k is the parameter updated iteratively during training, and $\tilde{\Lambda}$ is the rescaled eigenvalue matrix.

Substituting (6) into (5), we get the final graph convolution operation:

$$\begin{aligned} H^{l+1} &= \sigma(U(\sum_{k=0}^{K-1} \beta_k T_k(\tilde{\Lambda}))U^T H^l) \\ &= \sigma(\sum_{k=0}^{K-1} \beta_k T_k(U\tilde{\Lambda}U^T) H^l) \\ &= \sigma(\sum_{k=0}^{K-1} \beta_k T_k(\tilde{L}) H^l), \end{aligned} \tag{7}$$

where $\tilde{L} = 2L/\lambda_{\max} - I$ and $\lambda_{\max}$ is the maximum eigenvalue.

The edge weights are the weight inputs to the graph convolutional layers and help to dynamically adjust the importance of each edge. The hierarchical GCN model obtains the features of each layer and makes the features of different layers all contribute to the final classification. Finally, through the weighted splicing of the features of each layer, the model can fully integrate the global information, better extract the key features, and complete the final classification task.

E. Total Loss Function

In the population graph hierarchical graph neural network, we use the following cross-entropy loss function:

$$L_{CEL} = -\sum_{i=1}^{M}\sum_{c=1}^{C} y_{ic} \log \hat{y}_{ic}, \tag{8}$$

where C represents the number of classes, and y_{ic} and $\hat{y}_{ic}$ denote the ture and predicted labels of the ith subject belonging to the class $\{c, c = 1, 2, \cdots, C\}$, respectively.

Then, the total loss function L_{loss} of IPGNN is

$$L_{loss} = L_{CEL} + \alpha L_{MI}, \tag{9}$$

where α is the hyperparameter that balances these two terms.

III. EXPERIMENTS AND RESULTS

A. Dataset Preprocessing and Experimental Settings

We quantitatively evaluate our IPGNN model on the public Alzheimer's Disease Neuroimaging Initiative (ADNI) dataset [11]. 623 subjects are contained in our experiment, including 105 Alzheimer's disease (AD) patients, 169 Cognitively Normal (CN), 210 Early Mild Cognitive Impairment (EMCI), and 139 Late Mild Cognitive Impairment (LMCI). The basic information of the subjects is shown in Table I.

TABLE I: Data information used in ADNI experiments.

Clinical label	Number	Gender (F/M)	Age (Mean± Standard deviation)	Age (Max/Min)
EMCI	210	118/92	72.305±6.799	90/56
LMCI	139	55/84	72.014±7.779	88/57
AD	105	55/50	74.181±7.541	89/56
CN	169	95/74	75.142±6.380	96/65

All the fMRI data are acquired through a 3T Siemens Tim Trio whole-body scanner. The important scan parameters are as follows: TR (repetition time) = 3000 ms, TE (echo time) = 30 ms, matrix size = 64×64, flip angle = 80°, T = 140 volumes. The fMRI data are preprocessed using the preprocessing

TABLE II: Comparison of results of the binary classification experiment for AD and MCI. M(multimodal): × :uses only imaging data, ✓:uses both imaging and non-imaging data.

Methods	M	Subjects (Number)	Acc (Var)	Sen (Var)	Spe (Var)	AUC (Var)	F1 (Var)
BrainGNN [3]	×	AD (34) : MCI (100)	77.61 (4.30)	81.81 (3.09)	54.83 (3.69)	53.07 (5.65)	84.77 (2.01)
MVS-GCN [4]	×	AD (34) : MCI (99)	69.23 (4.32)	72.61 (3.26)	60.21 (2.74)	59.66 (5.43)	73.71 (2.69)
EV-GCN [6]	✓	AD (289) : MCI (251)	79.40	—	—	83.83	—
LG-GNN [7]	✓	AD (34) : MCI (100)	82.09 (1.40)	82.96 (0.91)	51.66 (4.84)	68.33 (3.47)	88.91 (1.12)
Proposed IPGNN	×	AD (105) : MCI (349)	**92.52 (0.09)**	**96.56 (0.11)**	**79.09 (2.29)**	**91.87 (0.43)**	**95.22 (0.03)**

TABLE III: Comparison of results of the binary classification experiment for MCI and CN.

Methods	M	Subjects (Number)	Acc (Var)	Sen (Var)	Spe (Var)	AUC (Var)	F1 (Var)
PopulationGCN [5]	✓	MCI (121) : CN (100)	67.41 (0.82)	**75.96 (1.33)**	57.00 (1.41)	62.34 (1.58)	71.65 (0.76)
InceptionGCN [13]	✓	MCI (121) : CN (100)	71.04 (1.12)	72.69 (2.66)	69.00 (1.29)	64.07 (1.50)	72.58 (1.57)
EV-GCN [6]	✓	MCI (121) : CN (100)	71.06 (0.81)	62.00 (6.36)	78.71 (1.91)	66.19 (1.49)	74.82 (0.54)
LG-GNN [7]	✓	MCI (121) : CN (100)	76.48 (0.44)	75.00 (2.45)	77.88 (1.20)	68.85 (1.33)	**78.23 (0.37)**
Proposed IPGNN	×	MCI (349) : CN (169)	**79.92 (0.11)**	62.87 (2.68)	**88.24 (0.68)**	**77.96 (0.28)**	66.30 (0.47)

TABLE IV: Comparison of results of the binary classification experiment for LMCI and EMCI.

Methods	M	Subjects (Number)	Acc (Var)	Sen (Var)	Spe (Var)	AUC (Var)	F1 (Var)
STNet [14]	×	LMCI (145) : EMCI (165)	79.36	80.95	77.00	83.21	—
Lei et al. [15]	×	LMCI (38) : EMCI (44)	81.71	78.95	**84.09**	**92.11**	—
Shao et al. [16]	×	LMCI (187) : EMCI (273)	75.48	83.84	63.26	71.00	—
song et al. [17]	✓	LMCI (38) : EMCI (44)	85.50	92.10	81.80	—	—
Proposed IPGNN	×	LMCI (139) : EMCI (210)	**87.39 (0.14)**	**93.33 (0.28)**	78.30 (0.90)	89.34 (0.15)	**89.90 (0.09)**

pipeline provided by SPM12 and the CONN Toolbox, the main steps of which include: realignment; motion estimation and slice correction; singularity detection; segmentation (grey matter/white matter/CSF) and normalisation to MNI (Montreal Neurological Institute) space; and spatial smoothing (6 mm full-width-half-maximum (FWHM) with a Gaussian kernel). Finally, the brain is partitioned into $N = 132$ ROIs based on the *in-built* atlas of the CONN toolbox. The BOLD time series of all voxels in each ROI are averaged to obtain the average time series for each ROI.

In the experiment, the loss function parameter α is set to be 0.01, the pooling ratio r is set to be 0.8, dropout is set to be 0.3, the maximum number of epochs is set to be 300, the Adam optimizer [12] with a learning rate of 0.01 is used, and the weight decay is 5×10^{-5}. The discriminator consists of a two-layer MLP and a sigmoid function. Ten-fold cross-validation is used to evaluate the datasets.

B. Quantitative Results

To validate the effectiveness of our IPGNN method, we report in this section the results of quantitative comparison of our model with other existing methods on the ADNI dataset. Five commonly used statistical metrics, namely accuracy (Acc), sensitivity (Sen), specificity (Spe), area under the curve (AUC) and F1 score, are used to evaluate the classification performance of the proposed framework network.

1) Binary classification experiment: As shown in Tables II, III and IV, we conduct three binary classification experiments, namely, AD vs. MCI (including LMCI and EMCI), MCI vs. NC, and LMCI vs. EMCI. In these three sets of experiments, the classification accuracy of our model reaches 92.52%, 79.92% and 87.39%, all of which are better than other existing methods, which demonstrates the effectiveness of our IPGNN model in classifying brain diseases.

2) Multi-classification experiment: We also conducted two multi-classification experiments: a three-classification experiment (AD vs. MCI vs. CN) and a four-classification experiment (AD vs. LMCI vs. EMCI vs. CN). Only one metric of accuracy is used for model evaluation. The results of the three- and four-classification experiments are shown in Tables V and VI, respectively, and the corresponding confusion matrices are shown in Fig. 4. The classification accuracy of the three-classification (AD vs. MCI vs. CN) is 75.12%, which is 3.36% higher than the existing algorithms. The classification accuracy of four-classification (AD vs. LMCI vs. EMCI vs. CN) is 66.61%, which is 5.94% better than the existing algorithms. These results further indicate that our IPGNN model outperforms other existing models.

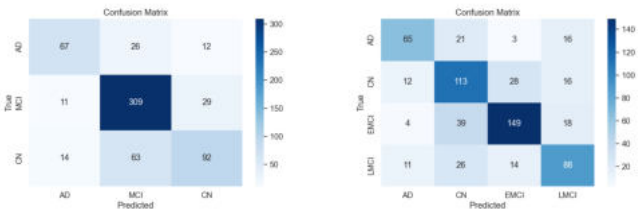

(a) AD:MCI:CN (b) AD:CN:EMCI:LMCI

Fig. 4: Visual view of the confusion matrix for multi-classification experiments of the ADNI dataset.

TABLE V: Comparison of results of the three-classification experiment of AD, MCI and CN.

Methods	Subjects (Number)	Acc
STNet [14]	AD (99) : MCI (310) : CN (164)	71.76
MRN [18]	AD (345) : MCI (613) : CN (360)	63.23
Proposed IPGNN	AD (105) : MCI (349) : CN (169)	**75.12**

TABLE VI: Comparison of results of the four-classification experiment of AD, LMCI, EMCI and CN.

Methods	Subjects (Number)	Acc
STNet [14]	AD (99) : LMCI (145) : EMCI(165) : CN (154)	60.67
wck-CN [19]	AD (31) : LMCI (45) : EMCI(50) : CN(48)	57.00
Proposed IPGNN	AD (105) : LMCI (139) : EMCI (210) : CN(169)	**66.61**

C. Detection of the Most Abnormal Brain Regions

In addition to quantitative experiments, we also conducted qualitative analyses to detect abnormal brain regions in AD patients to give the network interpretability. We calculate the top 15 most weighted brain regions for each subject, which are the most likely abnormal brain regions. The top 15 brain regions with the highest frequency of occurrence are analysed and brain maps are visualised using RESTplus and BrainNet Viewer. Fig. 5 shows the location of the most abnormal brain regions in patients under different experiments.

The experiments show that 1) With MCI as the control group, the abnormal brain regions in AD patients are mainly concentrated in the temporal pole (TP), precentral gyrus (PreCG), insular cortex (IC), superior frontal gyrus (SFG), hippocampus, central opercular cortex (CO), planum polare (PP), inferior frontal gyrus (IFG), lingual gyrus (LG), lateral occipital cortex (LOC), middle temporal gyrus (MTG), and cuneal cortex (Cuneal).

2) With CN as the control group, the abnormal brain regions in MCI patients are mainly concentrated in the temporal pole (TP), precentral gyrus (PreCG), parahippocampal gyrus (PaHC), cerebelum 3 (Cereb3), vermis 3 (Ver3), inferior temporal gyrus (ITG), intracalcarine cortex (ICC), middle frontal gyrus (MidFG), lingual gyrus (LG), superior frontal gyrus (SFG), and hippocampus.

3) With EMCI as the control group, the abnormal brain regions in LMCI patients are mainly concentrated in the lingual gyrus (LG), intracalcarine cortex (ICC), cuneal cortex (Cuneal), precentral gyrus (PreCG), supramarginal gyrus (SMG), supracalcarine cortex (SCC), insular cortex (IC), temporal occipital fusiform cortex (TOFusC), precuneous cortex (Precuneous), superior temporal gyrus (STG), Superior Parietal Lobule (SPL).

We compare the results of the qualitative analyses in this paper with existing findings and obtain that these regions, such as the lingual gyrus, precentral gyrus, hippocampus, insular cortex, frontal gyrus, and temporal gyrus, are the main abnormal brain regions in AD patients [20], [21]. It has been shown that changes in cortical morphometric information and wedge cortical thickness are accurate indicators of the conversion of MCI to AD [22], [23]. Liu et al. [24] found abnormalities in the inferior temporal gyrus, inferior occipital gyrus, postcentral gyrus, lingual gyrus, and anterior gyrus in MCI patients compared to NC. Lee et al. [25] found that LMCI patients had reduced functional connectivity in the precuneus, bilateral medial frontal gyrus and left angular gyrus compared to EMCI patients. Our findings are consistent with all of these reports, demonstrating that our proposed IPGNN model not only achieves high-precision classification, but also reliably extracts abnormal brain regions in AD patients.

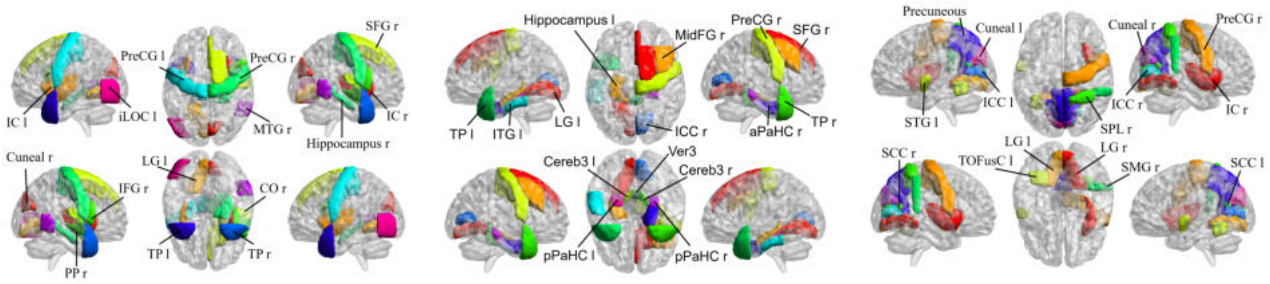

(a) AD vs. MCI (b) MCI vs. CN (c) LMCI vs. EMCI

Fig. 5: The top 15 abnormal brain areas a) AD patients, b) MCI patients, and c) LMCI patients.

IV. Conclusion

In this paper, we have fused the information from individual and population graphs to propose a new graph neural network model for brain disease diagnosis - IPGNN. We have processed the fMRI data through an individual graph coarsening network to obtain the most representative coarsened features, and then fused these features as node features into a population graph, and introduced the HOFC graph metrics as edge weights of the population graph to measure the similarity between subjects. We have conducted several binary and multiclassification experiments on the public ADNI dataset, and the results show that our proposed IPGNN model has excellent recognition performance for AD and MCI. In addition, the model can be used for the detection of abnormal brain regions to assist in disease diagnosis and provide interpretable analyses for the classification results. By fusing individual and population graphs, the IPGNN model overcomes the limitations of individual graph-based brain networks in ignoring the relationships between subjects and the difficulties in detecting abnormal brain regions in population graph-based brain networks, effectively improving the performance of the model. In this work, we analyse and process the functional connections between pairs of brain regions. Future work can explore more complex and deeper connections between multiple brain regions and build a hypergraph neural network. And more information can be incorporated into the learning, such as non-imaging information.

Acknowledgment

This work was supported by the National Nature Science Foundation of China (grants 62176192, 62173259 and 62101392).

References

[1] T. N. Kipf and M. Welling, "Semi-supervised classification with graph convolutional networks," *arXiv preprint arXiv:1609.02907*, 2016.

[2] P. Veličković, G. Cucurull, A. Casanova, A. Romero, P. Lio, and Y. Bengio, "Graph attention networks," *arXiv preprint arXiv:1710.10903*, 2017.

[3] X. Li, Y. Zhou, N. Dvornek, M. Zhang, S. Gao, J. Zhuang, D. Scheinost, L. H. Staib, P. Ventola, and J. S. Duncan, "BrainGNN: Interpretable brain graph neural network for fmri analysis," *Medical Image Analysis*, vol. 74, p. 102233, 2021.

[4] G. Wen, P. Cao, H. Bao, W. Yang, T. Zheng, and O. Zaiane, "MVS-GCN: A prior brain structure learning-guided multi-view graph convolution network for autism spectrum disorder diagnosis," *Computers in Biology and Medicine*, vol. 142, p. 105239, 2022.

[5] S. Parisot, S. I. Ktena, E. Ferrante, M. Lee, R. G. Moreno, B. Glocker, and D. Rueckert, "Spectral graph convolutions for population-based disease prediction," in *Medical Image Computing and Computer Assisted Intervention- MICCAI 2017: 20th International Conference, Quebec City, QC, Canada, September 11-13, 2017, Proceedings, Part III 20*. Springer, 2017, pp. 177–185.

[6] Y. Huang and A. C. Chung, "Disease prediction with edge-variational graph convolutional networks," *Medical Image Analysis*, vol. 77, p. 102375, 2022.

[7] H. Zhang, R. Song, L. Wang, L. Zhang, D. Wang, C. Wang, and W. Zhang, "Classification of brain disorders in rs-fMRI via local-to-global graph neural networks," *IEEE Transactions on Medical Imaging*, vol. 42, no. 2, pp. 444–455, 2022.

[8] H. Zhang, P. Giannakopoulos, S. Haller, S.-W. Lee, S. Qiu, and D. Shen, "Inter-network high-order functional connectivity (IN-HOFC) and its alteration in patients with mild cognitive impairment," *Neuroinformatics*, vol. 17, pp. 547–561, 2019.

[9] Y. Pang, Y. Zhao, and D. Li, "Graph pooling via coarsened graph infomax," in *Proceedings of the 44th International ACM SIGIR Conference on Research and Development in Information Retrieval*, 2021, pp. 2177–2181.

[10] Z. Gao, Z. Lu, J. Wang, S. Ying, and J. Shi, "A convolutional neural network and graph convolutional network based framework for classification of breast histopathological images," *IEEE Journal of Biomedical and Health Informatics*, vol. 26, no. 7, pp. 3163–3173, 2022.

[11] ADNI Dataset. [Online]. Available: https://ida.loni.usc.edu/

[12] D. P. Kingma and J. Ba, "Adam: A method for stochastic optimization," *arXiv preprint arXiv:1412.6980*, 2014.

[13] A. Kazi, S. Shekarforoush, S. Arvind Krishna, H. Burwinkel, G. Vivar, K. Kortüm, S.-A. Ahmadi, S. Albarqouni, and N. Navab, "InceptionGCN: receptive field aware graph convolutional network for disease prediction," in *Information Processing in Medical Imaging: 26th International Conference, IPMI 2019, Hong Kong, China, June 2–7, 2019, Proceedings 26*. Springer, 2019, pp. 73–85.

[14] M. Wang, C. Lian, D. Yao, D. Zhang, M. Liu, and D. Shen, "Spatial-temporal dependency modeling and network hub detection for functional MRI analysis via convolutional-recurrent network," *IEEE Transactions on Biomedical Engineering*, vol. 67, no. 8, pp. 2241–2252, 2019.

[15] B. Lei, N. Cheng, A. F. Frangi, E.-L. Tan, J. Cao, P. Yang, A. Elazab, J. Du, Y. Xu, and T. Wang, "Self-calibrated brain network estimation and joint non-convex multi-task learning for identification of early Alzheimer's disease," *Medical image analysis*, vol. 61, p. 101652, 2020.

[16] W. Shao, Y. Peng, C. Zu, M. Wang, D. Zhang, A. D. N. Initiative *et al.*, "Hypergraph based multi-task feature selection for multimodal classification of Alzheimer's disease," *Computerized Medical Imaging and Graphics*, vol. 80, p. 101663, 2020.

[17] X. Song, F. Zhou, A. F. Frangi, J. Cao, X. Xiao, Y. Lei, T. Wang, and B. Lei, "Graph convolution network with similarity awareness and adaptive calibration for disease-induced deterioration prediction," *Medical Image Analysis*, vol. 69, p. 101947, 2021.

[18] J. Zhang, X. He, L. Qing, X. Chen, Y. Liu, and H. Chen, "Multi-relation graph convolutional network for Alzheimer's disease diagnosis using structural MRI," *Knowledge-Based Systems*, vol. 270, p. 110546, 2023.

[19] B. Jie, M. Liu, C. Lian, F. Shi, and D. Shen, "Designing weighted correlation kernels in convolutional neural networks for functional connectivity based brain disease diagnosis," *Medical image analysis*, vol. 63, p. 101709, 2020.

[20] G. Halliday, "Pathology and hippocampal atrophy in Alzheimer's disease," *The Lancet Neurology*, vol. 16, no. 11, pp. 862–864, 2017.

[21] E. McLachlan, J. Bousfield, R. Howard, and S. Reeves, "Reduced parahippocampal volume and psychosis symptoms in Alzheimer's disease," *International Journal of Geriatric Psychiatry*, vol. 33, no. 2, pp. 389–395, 2018.

[22] C.-Y. Wee, P.-T. Yap, D. Shen, and A. D. N. Initiative, "Prediction of Alzheimer's disease and mild cognitive impairment using cortical morphological patterns," *Human brain mapping*, vol. 34, no. 12, pp. 3411–3425, 2013.

[23] E. Niskanen, M. Könönen, S. Määttä, M. Hallikainen, M. Kivipelto, S. Casarotto, M. Massimini, R. Vanninen, E. Mervaala, J. Karhu *et al.*, "New insights into Alzheimer's disease progression: a combined TMS and structural MRI study," *PLoS One*, vol. 6, no. 10, p. e26113, 2011.

[24] R. Liu, B. Hu, Z. Yao, M. Ratcliffe, W. Wang, C. Liang, Q. Cai, J. Yang, and Q. Zhao, "Abnormal neural activity and functional connectivity in amnestic Mild cognitive impairmet: A resting state fMRI study," in *2013 6th International IEEE/EMBS Conference on Neural Engineering (NER)*. IEEE, 2013, pp. 765–769.

[25] E.-S. Lee, K. Yoo, Y.-B. Lee, J. Chung, J.-E. Lim, B. Yoon, Y. Jeong, A. D. N. Initiative *et al.*, "Default mode network functional connectivity in early and late mild cognitive impairment: results from the Alzheimer's disease neuroimaging initiative," *Alzheimer Disease & Associated Disorders*, vol. 30, no. 4, pp. 289–296, 2016.